applied sciences

MDPI

Article

Microstructural Evolution within the Interphase between Hardening Overlay and Existing Concrete Substrates

Łukasz Sadowski * and Damian Stefaniuk

Faculty of Civil Engineering, Wrocław University of Science and Technology, Wybrzeże Wyspiańskiego 27, 50-370 Wrocław, Poland; damian.stefaniuk@pwr.edu.pl

* Correspondence: lukasz.sadowski@pwr.edu.pl; Tel.: +48-71-320-37-42

Academic Editor: Jorge de Brito

Received: 23 December 2016; Accepted: 23 January 2017; Published: 25 January 2017

Abstract: This article presents the microstructural evolution within the interphase between a hardening overlay made of cement mortar and an existing concrete substrate. The substrate has been treated using four methods, due to which different surfaces were obtained: a raw surface, a surface formed after contact with the formwork, a grinded surface, and a shotblasted surface. Special focus is placed on the results of the microporosity within the interphase zone (IZ) using X-ray micro computed tomography (micro-CT). The microporosity profiles obtained from the micro-CT images have been used to assess the nature of the IZ between the hardening overlay and the existing concrete substrate. It has been shown that microporosity and the number of pores in the concrete within the IZ increases during the hardening time of an overlay made of cement mortar. It also depends on the applied surface treatment method. However, no significant changes in the microporosity of the existing concrete substrate have been noted.

Keywords: concrete; surface treatment; cement mortar; overlay; substrate; microporosity; microstructure; interface; interphase; X-ray micro computed tomography

1. Introduction

In civil engineering, overlay (also known as top layer, coating, added layer or topping) can be defined as a layer with variable thickness that is placed on an existing concrete substrate. Overlay allows the specific functional performance of civil engineering structures, such as noisiness or anti-corrosion treatments, to be obtained [1–3]. It is usually made of concrete or cement mortar. However, its durability substantially depends on the proper adhesion to the existing concrete substrate. Courard [4] distinguished specific adhesion, which is related to chemical and physicochemical interactions, and mechanical adhesion due to the mechanical interlocking. According to Czarnecki and Chmielewska [5], the level of adhesion is affected by the compressive strength, temperature, and humidity of the existing concrete substrate.

According to Bissonnette et al. [6], as a result of hardening of the material of the overlay laid on an existing concrete substrate, an interphase is formed. It is different from the interface formed at the time of laying the overlay. The interphase, which is the border between two phases, becomes less evident after contact is made because the hardening overlay is interconnected with the existing concrete substrate. Thus, according to [7], a zone with noticeable changes in microstructure with a thickness of 1 mm to 2 mm can be termed the interphase zone (IZ) when considering porosity.

The microstructural properties, specifically the porosity within the IZ, determine the performance and durability of multi-layer concrete structures. The concrete within the IZ between the overlay and the existing concrete substrate is heterogeneous and porous in different scales of observations.

Therefore, it is difficult to correctly characterize it from a microstructural point of view. Understanding and analyzing the origin of its heterogeneity is the subject of microstructural evolution with regard to the context of phase transformation of concrete within the IZ. Knowledge of this evolution, together with the short-term and long-term performance of the water-to-cement ratio of the overlays during hardening, is essential and remains a challenging task [8–12]. As mentioned in [13,14], the material within the IZ between the overlay and existing substrate usually has a different aggregate/cement content, w/c ratio, and temperature during the hardening period. Therefore, processes for creating the microstructure within the IZ between a hardening overlay and the existing concrete substrate are crucial. Thus, the investigation of the evolution of the microstructure within the IZ, as a result of specific surface treatment, remains difficult [15].

As mentioned by Sierra-Beltran et al. [16], the early-age shrinkage deformation of the material of the overlay is restrained by the existing concrete substrate that has already undergone shrinkage. It is because a combination of tensile and shear stresses built up along the interface [16]. Moreover, the physical properties of the interlocked materials, such as viscosity and wettability, are crucial in understanding the adhesion phenomena [17–19]. Lukovic and Ye [20] stated that the material properties of the overlay and the IZ are greatly influenced by the moisture exchange between the overlay and existing substrate, which affects pore structure development [21,22]. The porosity, morphology, and microcracking of the concrete substrate have a significant effect on the adhesion level [23–29]. Stolz et al. [30] stated that increasing the real (effective) contact area between the existing concrete substrate and the overlay, as a result of different surface textures, does not always increase the interlayer bond. On the other hand, the rheology of the hardening overlay seems to be the main factor influencing the adhesion [30]. As mentioned by Halicka and Franczak [31], the adhesion level between hardening overlay and substrate usually increases with time. However, there is still a lack of knowledge of the evolution of the microstructural properties of the IZ between hardening overlay and substrate.

Scanning electron microscopy (SEM) used to play a major role in the evaluation of the microstructure of the concrete within the IZ [32–40]. These tests were mostly qualitative and evaluated on a hardened overlay. Recently, Luković et al. [41] used nanoindentation to study the micromechanical interface properties in a concrete repair system. However, these methods need specific preparation of a sample. SEM is very invasive and includes cutting, polishing, and exposure to high vacuum pressure inside the chamber and can also modify the microstructure of the sample [42]. It masks a thoughtful problem in hardening samples. The processes of the microstructural evolution within the IZ during hardening are still not fully understood because of the limitations of available test methods.

Currently, the evolution of material properties over time is attracting the attention of researchers [43–45]. Understanding the microstructural evolution in concrete and cement paste during hardening is a very challenging issue. Recently, He et al. [46], Helfen et al. [47], and Sun et al. [48] used high resolution X-ray micro-computed tomography (micro-CT) for this purpose. This advanced technique has been proven to provide information on the real size and spatial distribution of the pores, which cannot be obtained by classical techniques [49–54]. Parisatto et al. [42] pointed out that no other experimental technique is presently capable of non-invasive high resolution imaging such a complex microstructure in 3D with submicrometric resolution in a non-invasive manner. Recently, micro-CT has become a popular tool for the evaluation of concrete and cement mortar porosity [55–59]. However, most of the studies have been carried out on hardened concrete. To the best of our knowledge, there are no studies in the literature that evaluate the microstructural changes within the IZ between the hardening overlay made of cement mortar and the existing concrete substrate.

Therefore, the aim of this paper is to evaluate the microstructural evolution within the interphase between the hardening overlay made of cement mortar and the existing concrete substrate for different concrete substrate surface treatments. In order to better understand this complex process, the microstructure will be compared at different stages of overlay hardening. To characterize the microstructure of the mortar and concrete, micro-CT will be used. The microporosity profiles obtained from the processing of micro-CT images will be used to assess the nature of the IZ between a hardening

overlay and existing substrate. The paper is organized as follows: Section 2 presents the description of research problems with their background, materials and methods used, and data acquisition; Section 3 condenses the analysis of results; and Section 4 presents conclusions and a discussion.

2. Materials and Methods

The investigated elements were made from the substrate and the overlay. The substrate was made from concrete with a maximum aggregate grain size of 8 mm. The constituents of the concrete (Dyckerhoff Poland, Wrocław, Poland) used to make the substrate were ($/m^3$) as follows: 352 kg of type II A-LL 42.5 R Portland cement, 165 L of water, 724.4 kg of fine aggregate with a 1.53 fineness modulus and a seed density of 2.60 Mg/m^3, 1086.6 kg of crushed basalt aggregates with a 4.51 fineness modulus and a seed density of 2.62 Mg/m^3, and 40 kg of fly ash. The 2.0 L of plasticizer Sika® ViscoFlow®-6920 (Sika Poland, Warsaw, Poland), based on polycarboxylates with a density of 1.07 g/cm^3, was used to achieve a workable condition of the substrate concrete mixture. The substrate was cured naturally at an air temperature of +20 °C (±2 °C) and an air relative humidity of 65% (±5%). In order to diversify the surface morphology, when the concrete substrate attained 28 days of age, the concrete substrate surface of the specimen was treated. Based on the literature survey, four different surface treatment methods were selected. This resulted in four different concrete surface morphologies (Figure 1). The first surface (T1—raw) was not specially treated, but only path grabbed, which is in practice the most popular method. The second (T2—as cast) was also not specially treated, but was formed after contact with the formwork. The third surface (T3—ground) was mechanically treated using a hand-held angle grinder with an abrasive disc and dust removal. The fourth surface (T4) was shotblasted using a lightweight shotblasting system with a buckshot diameter of 6 mm after the removal of dust.

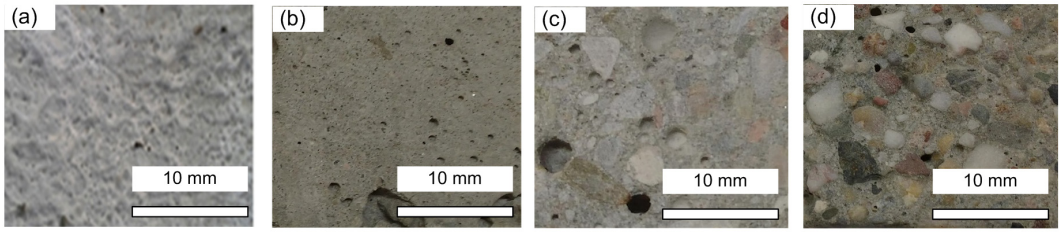

Figure 1. Optical views of the differently treated concrete surfaces: (**a**) raw; (**b**) as cast; (**c**) ground; (**d**) shotblasted.

From the differently treated concrete substrates, cylindrical samples were cut (20 mm in diameter and 25 mm in thickness). An overlay with a thickness of 25 mm was laid on the existing concrete substrate surfaces. The overlay was made from cement mortar with a maximum aggregate grain size of 2 mm. The constituents of the cement mortar used to make the overlay were ($/m^3$) as follows: 276 kg of type I R Portland cement, 138 L of water and 1599.0 kg of fine aggregate with a 1.53 fineness modulus and a seed density of 2.60 Mg/m^3. The overlay hardened in a moist chamber. For the micro-CT investigation, the test specimens were put into a closed holder and wrapped in PVC film in order to keep a constant moisture content for the testing (at 3 h, 1 day, 3 days, and 28 days). Finally, the samples with a diameter of 20 mm and thickness of 50 mm were subjected to tests (Figure 2). The substrate as well as the overlay had a thickness of 25 mm (Figure 2b).

The equipment used for obtaining the 3D images of the samples' microstructure was an X-ray micro-CT scanner with a resolution of 11 Mp (SkyScan 1172, Bruker microCT, Kontich, Belgium), presented in Figure 2a. In this scanner model, an X-ray tube operates within a voltage range of 20–100 kV and a power of up to 10 W. To obtain the images, the energy of the incident X-ray beam was set to 100 kV and Al + Cu filters were used. Based on the applied energy, a good balance between X-ray penetration and absorption contrast can be obtained. An angle rotation of up to 360° was adopted at 0.35° steps with a resolution of 8 µm/px (micrometer per pixel). For each tomographic scan, 1028 X-ray

projections were acquired. Raw projection data was collected using the fully distortion-corrected 11 Mp X-ray camera, which is a 12-bit cooled charge coupled device (CCD) fiber-optical camera that is coupled to a scintillator.

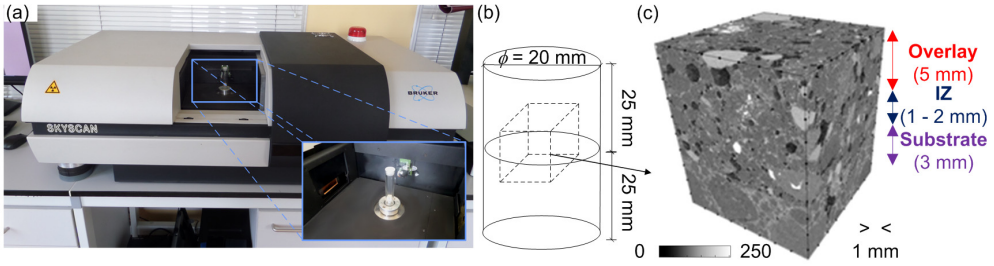

Figure 2. View of (**a**) the X-ray micro-CT (micro-computed tomography) with a sample placed on a tripod; (**b**) the scheme of the sample element prepared for tests using the micro-CT method; (**c**) a fragment of the 3D image of a microstructure subjected to further analysis.

To analyze the microstructural evolution within the interphase between the hardening overlay made of cement mortar and the existing concrete substrate, the exposure time was kept as low as possible in order to reduce the total duration of the experiments. Using the described setup, each scan took approximately 110–120 min. It was an acceptable timescale for the study of the microporosity changes in the concrete within the interface. Thus, the measured microporosity value is the average of this time period. An initial attempt to scan a sample just after preparation gave unsatisfactory results, which was due to a faster evolution of the microstructure than the scanning time. A decrease in the total scan duration is possible by reducing the exposure time and the number of projections, although this would result in increased artefacts and reduced contrast in the reconstructed images. Therefore, the scanning parameters were chosen in order to minimize the scan duration while at the same time keeping a sufficiently high quality of the images. In addition, the short scanning time allowed a reduction of the thermal load to the sample due to the higher temperature in the micro-CT chamber during the scan compared with the ambient temperature (up to 28 °C). This minimized water evaporation and unnatural changes within the fresh paste. A reconstruction of the obtained projections was made using NRecon 1 (Version 1.7.0.4, SkyScan, Kontich, Belgium) based on the Feldkamp algorithm [60]. To analyze the same test specimen at different time periods, it is important to use the same parameters during the scanning and reconstruction. After reconstruction, the 3D images were set together according to the reference scan (at 3 h) using 3D registration in DataViewer 1 (Version 1.5.2.4, SkyScan, Kontich, Belgium).

In order to avoid the boundary effect [61], only a part of the 3D image was used for further analysis in CTAnalyzer 1 (Version 1.16, SkyScan, Kontich, Belgium). The microstructural changes occurring within a volume of interest (VOI) were evaluated by analyzing the same portion of each sample at different ages and then comparing the variations of microporosity in the tomographic images along the sample height. For that purpose, rectangular VOIs were accurately selected at identical positions from each 3D dataset. The width of the VOIs was equal to 1000 × 1000 voxels (voxel size = 8.0 µm), while the vertical extent was limited to 1250 slices. From a statistical point of view, the examined volumes can be considered representative for the overlay (the main objective of this study), taking into account the size of the air voids and aggregates in the overlay. The porosity analysis was followed by filtering and binarization of the images for a predetermined threshold value (the same for all scans), due to which it was possible to calculate the microporosity ϕ defined as

$$\phi = \frac{V_V}{V_T} \quad (1)$$

where V_V is the volume of void-space (micropores), and V_T is the total or bulk volume of material, including the solid and void components.

Due to the size of the sample and the duration of the measurement, the obtained resolution only allows microporosity to be measured. Gallucci et al. [62] clearly showed that the measured porosity content and pore connectivity are strongly affected by the voxel size, and in particular that the segmented porosity decreases with increasing voxel size. Thus, the obtained values of microporosity will be lower compared to the overall macroscopic porosity values.

The detailed methodology applied for the microstructural evolution analyses within the IZ between the hardening overlay made of cement mortar and the existing concrete substrate using the micro-CT method is presented in Figure 3.

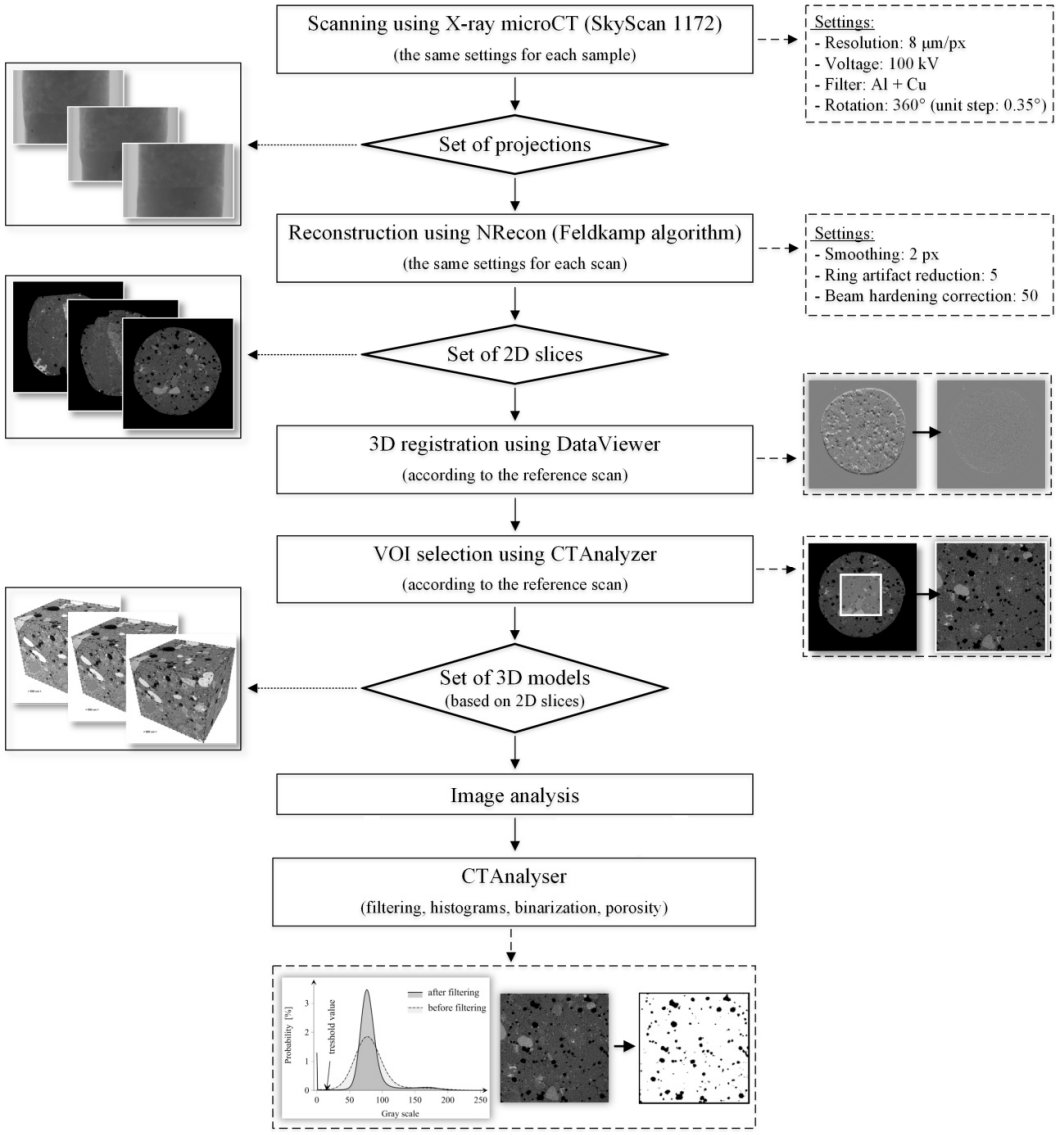

Figure 3. Methodology applied for microstructural evolution within the IZ (interphase zone) between the hardening overlay made of cement mortar and the existing concrete substrate using the micro-CT method.

3. Results

Exemplary 2D microstructure views of Samples T1, T2, T3, and T4, obtained on the basis of tests using the micro-CT method at 28 days, are shown in Figure 4.

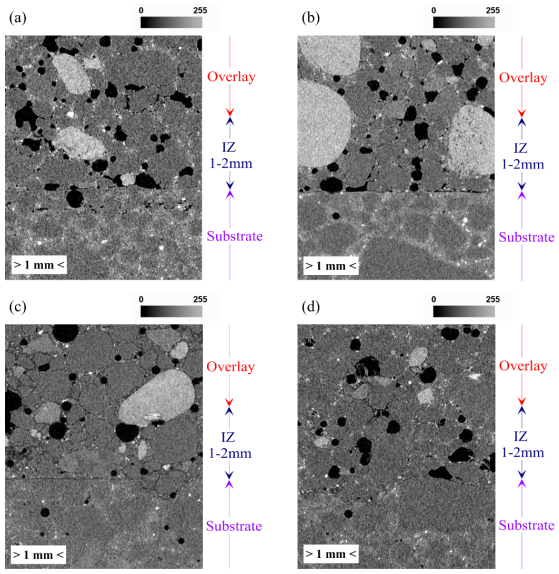

Figure 4. 2D microstructure views of the IZ between the overlay made of cement mortar and the existing concrete substrate obtained using the micro-CT method at 28 days of hardening of the overlay for Samples (**a**) T1; (**b**) T2; (**c**) T3; and (**d**) T4.

From the 2D microstructure views presented in Figure 4, it can be seen that there are noticeable differences in the microstructure within the IZ for differently treated concrete substrates. The microstructure within the IZ for raw concrete substrate has small cracks and a higher porosity of the near-surface zone of the concrete substrate (Figure 4a). It can be caused by patch grabbing of the surface of the fresh concrete that was used to obtain the raw surface of the hardened concrete substrate. For smooth concrete substrates formed after contact with the formwork (Figure 4b) or after grinding (Figure 4c) at 28 days of hardening of the overlay, a straight line with a higher porosity between the overlay and the existing concrete substrate can be seen. Within the IZ between the overlay and shotblasted concrete substrates, the microstructural changes are small. This may be caused by the fact that shotblasting usually allows higher adhesion between the layers to be obtained compared with other surface treatment methods. These issues may be related to the microporosity changes within the IZ, which can differ for different surface treatment methods. To analyze this phenomenon, Figure 5 presents the 3D models of the porosity of Samples T1–T4. Based on the qualitative visual assessment of the 3D porosity models, it can be noticed that the overlay and the existing concrete substrate are made of materials with a significantly different porosity (especially microporosity). The porosity of the cement mortar used to make the overlay is much higher than that for the concrete used to make the existing concrete substrate. This is due to the mix design and the method of concreting. Thanks to the difference of the porosity between the examined materials, the changes of the porosity within the IZ may be visible. However, the results cannot be assumed for all the other mix designs. For the shotblasted concrete substrate (Figure 5d), the porosity of the substrate is higher than that for surfaces treated with different methods. This can be a result of shotblasting. Therefore, it is of interest of how and if the microporosity changes at different moments within the IZ between the hardening overlay and the existing concrete substrate, and for different surface treatment methods. The IZ has been distinguished from the overlay with a thickness of 1 mm to 2 mm. This range has been found in [7] to be appropriate for this material configuration. Based on this analysis, it seems necessary to examine the microporosity ϕ and the number of pores n as a function along a sample height obtained within the IZ between the overlay and the existing concrete substrate using the micro-CT method at different moments of hardening of the overlay. The changes were noted at 3 h, 1 day, 3 days, and 28 days of overlay hardening.

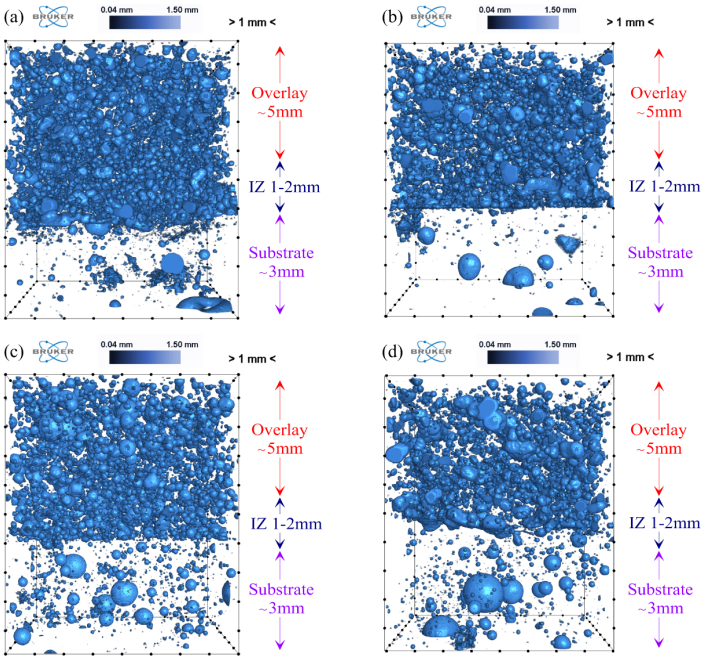

Figure 5. The 3D models of microporosity obtained within the IZ between the overlay made of cement mortar and the existing concrete obtained by the micro-CT method at different moments of overlay hardening for Samples (**a**) T1; (**b**) T2; (**c**) T3; and (**d**) T4.

Microporosity ϕ and the number of pores *n* within the IZ between the overlay and the existing concrete substrate, obtained using the micro-CT method, are formed as a function along the height of the sample (Figures 6 and 7). The results at four different moments of testing time are set together, and it can be seen that the changes are visible. However, the changes are only visible in the overlay and IZ between the layers, and not for the existing concrete substrate.

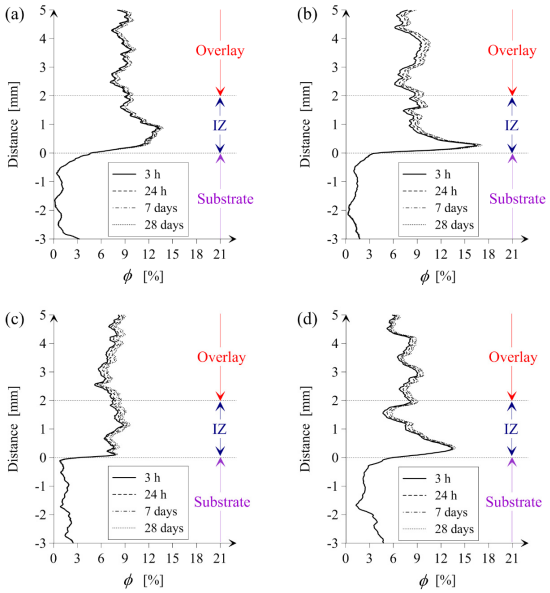

Figure 6. The microporosity ϕ as a function along a sample height obtained within the IZ between the overlay made of cement mortar and the existing concrete substrate obtained using the micro-CT method at different moments of overlay hardening for Samples (**a**) T1; (**b**) T2; (**c**) T3; and (**d**) T4.

It can be seen from Figure 6 that the microporosity at different moments of hardening of the overlay increases with time. It can be noted that only the microporosity, thanks to micro-CT, has been calculated. Based on the variation of the microporosity along the sample height, a different thickness of the IZ could be adopted for different surface treatment methods (Figure 6). Even though the differences are apparent, when comparing for further analysis, the IZ zone with a width of 2 mm was adopted. It is also visible that the microporosity ϕ within the IZ, except for T3 with the ground concrete substrate (Figure 6c), is much higher than that within the overlay for most of the specimens. The highest changes between the microporosity of the overlay and microporosity within the IZ are visible for Sample T2 for the as-cast concrete substrate (Figure 6b) and the shotblasted concrete substrate (Figure 6d).

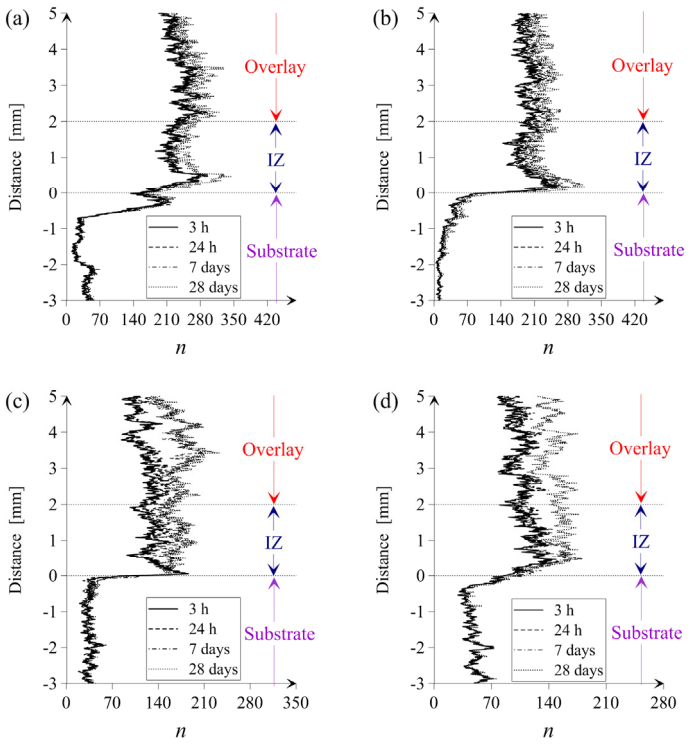

Figure 7. The number of pores n as a function along a sample height obtained within the IZ between the overlay made of cement mortar and the existing concrete substrate obtained by the micro-CT method at different moments of overlay hardening for Samples (**a**) T1; (**b**) T2; (**c**) T3; and (**d**) T4.

It can be seen in Figure 7 that the number of pores n at different moments of hardening of the overlay increases with time. It is much more visible for Samples T3 and T4, where mechanical surface treatment has been applied. For Samples T1 and T2 (without special surface treatment), the changes are insignificant. It is visible that the number of pores at 28 days of hardening of the overlay for samples within the IZ is similar to the number of pores in the overlay. However, at 3 h of hardening of the overlay for Samples T3 and T4 (Figure 7c–d), the number of pores is higher at the IZ than within the overlay. Additional analyses, however, did not show any changes in the shape of the pores during time. In Figure 8, the change in microporosity ϕ as a function along a sample height obtained within the IZ between the overlay and the existing concrete substrate is presented. This change was obtained using the micro-CT method at different moments of hardening of the overlay.

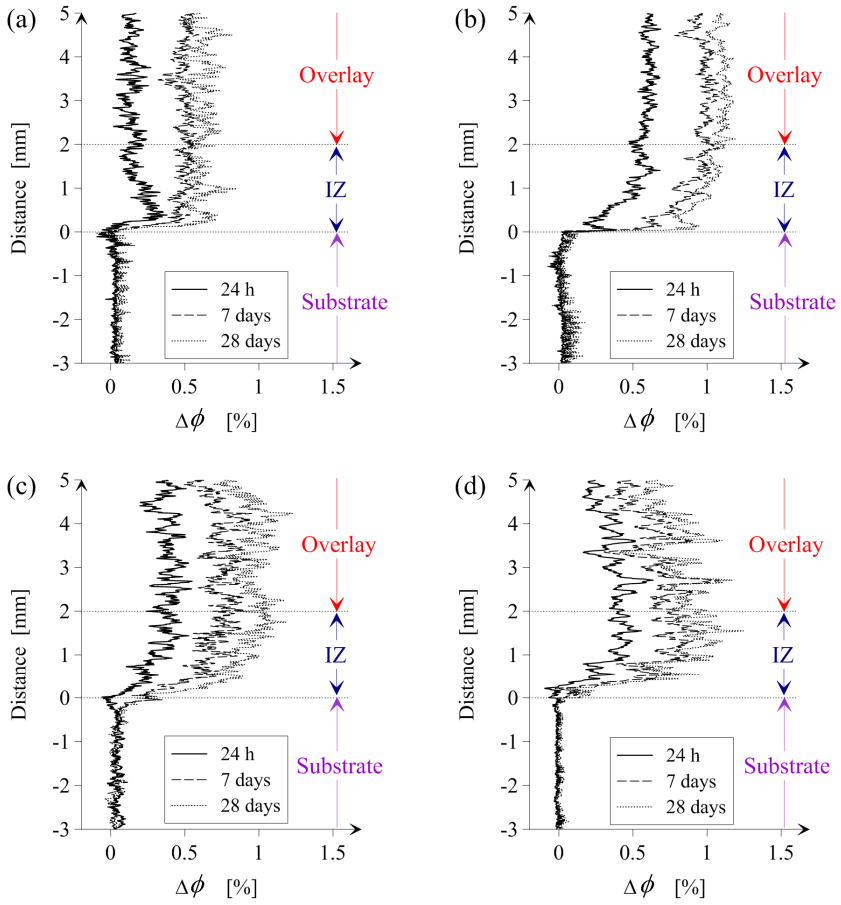

Figure 8. The change in microporosity ϕ as a function along a sample height obtained within the IZ between the overlay made of cement mortar and the existing concrete substrate obtained using the micro-CT method at different moments of hardening of the overlay for Samples (**a**) T1; (**b**) T2; (**c**) T3; and (**d**) T4.

As can be seen in Figure 8, after the first scan at 3 h of hardening of the overlay, the change in microporosity between the overlay and the substrate in the IZ differ and depend on the surface treatment of the existing concrete substrate. There are no significant changes in the microporosity of the existing concrete substrate. The greatest changes, related to the first scan performed after 3 h, can be seen at 28 days of hardening of the overlay. For Sample T1, the microporosity increases by around 0.7%, while for the other samples the increase is higher than 1% after the first scan at 3 h of hardening of the concrete overlay. Taking the above into consideration, Figure 9 presents the average microporosity ϕ as a function along a sample height obtained within the IZ between the overlay and the existing concrete substrate using the micro-CT method at different moments of hardening of the overlay.

It can be seen in Figure 9 that a major jump in the microstructural evolution occurs at between 3 and 24 h, which can be accompanied with the rapid development of hydration. In addition, the average microporosity ϕ is higher within the IZ than that within the overlay for all samples. The highest difference is for the concrete substrate surfaces without special surface treatment (Figure 9a,b). The lowest difference is for the ground surface of the existing concrete substrate (Figure 9c).

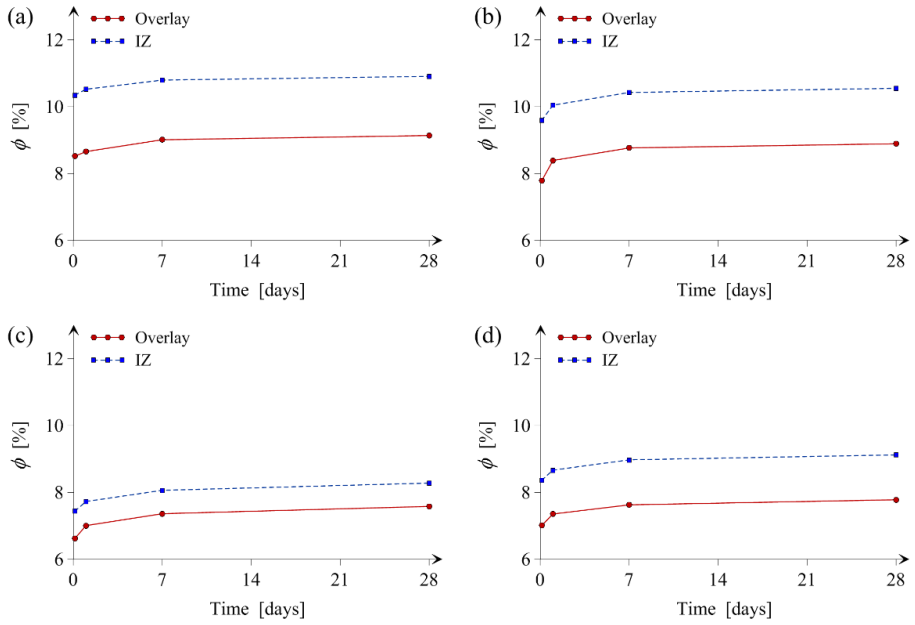

Figure 9. The average microporosity ϕ as a function along a sample height obtained within the IZ between the overlay and the existing concrete substrate obtained using the micro-CT method at different moments of overlay hardening for Samples (**a**) T1; (**b**) T2; (**c**) T3; and (**d**) T4.

It can be seen in Figure 10 that the average number of pores *n* within the IZ is higher than that obtained within the overlay for as-cast (Figure 10b) and shotblasted (Figure 10d) concrete substrates. On the other hand, for raw concrete substrate (Figure 10a) and ground concrete substrate (Figure 10c), the average number of pores *n* within the overlay is higher than that obtained within the IZ. This exception has been noted for ground concrete substrate for the first scan (after 3 h).

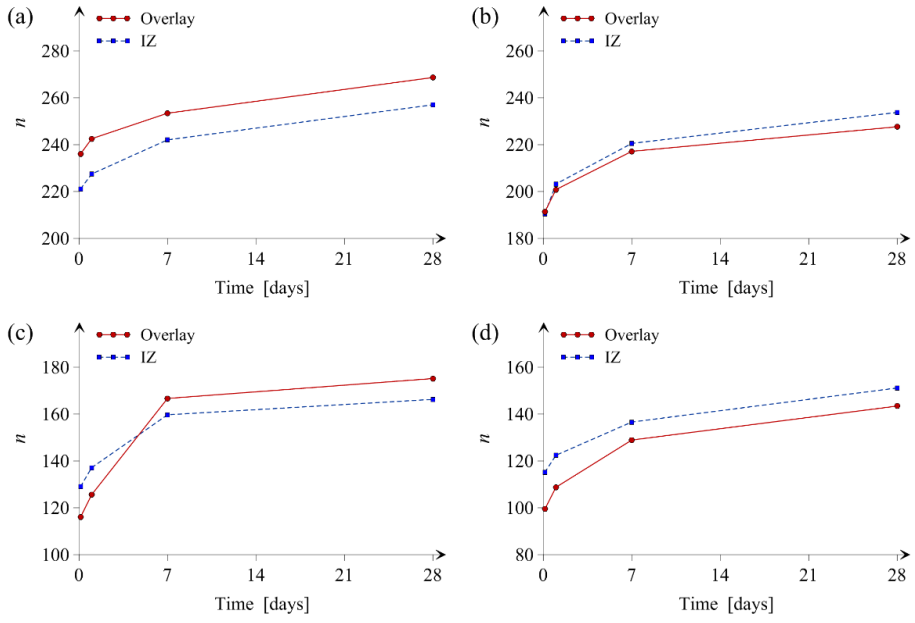

Figure 10. The average number of pores *n* as a function along a sample height obtained for the concrete within the IZ between the overlay and the existing concrete substrate obtained using the micro-CT method at different moments of overlay hardening for Samples (**a**) T1; (**b**) T2; (**c**) T3; and (**d**) T4.

4. Conclusions and Discussion

In the approach presented in this article, microporosity tests were performed to study the microstructural evolution of the interphase between hardening overlay and existing concrete substrate. Based on the presented research, the following conclusions can be drawn:

- The results presented in this work confirm the potential of high resolution X-ray micro-CT to observe the microstructural evolution within the interphase between hardening mortar and existing concrete substrate. A simple methodology was illustrated. If carefully applied, the procedure is a useful tool for evaluating the microstructural features within the IZ.
- The average values of microporosity within the IZ differ in relation to the microporosity in the hardening overlay. The highest difference is for surfaces without special surface treatment (T1 and T2), and the lowest for ground surfaces (T3). There are no significant changes in the microporosity of the concrete in the existing substrate.
- The average number of pores increases within the IZ at different moments of hardening of the overlay. It is much more observable for Samples T3 and T4, where mechanical surface treatment has been applied. The number of pores at 28 days of hardening of the overlay for samples within the IZ is similar to the number of pores in the overlay.
- Due to the size of the sample and the duration of the test, the obtained resolution allows microporosity to be measured. Thus, the obtained values of microporosity will be lower compared to the overall macroscopic porosity values.
- The number of micropores exhibits a more progressive increase than the microporosity. It could be due to the fact that more new micropores appear later. Their volume is small when compared to the overall volume of micropores. Later, the changes in morphology of the smaller pores could still occur at a lower scale of observation, while the changes in morphology of the greater pores at a higher scale are not meaningful.
- If microporosity is increasing, it is likely that changes could also occur in nanoporosity. This is evidenced by the latest test using mercury intrusion porosimetry (MIP), which is presented in [63]. However, we are not able to verify it using micro-CT because of the available resolution and required size of the sample.
- Based on the variation of the microporosity along the sample height, a different thickness of the IZ can be adopted for different surface treatment methods. The thickness of the IZ cannot be constant and depends on the mix design and existing concrete substrate surface condition and may be influenced by the overlay properties (thickness, aggregate size, etc.).
- This approach does not cover the pull-off adhesion between mortar and existing concrete substrate. It does, however, give the strength of the IZ between the hardening overlay and the existing concrete substrate, which is quantified by microporosity measurements.

Moreover, critical aspects related to sample preparation and experimental conditions have to be discussed. The main technical limitation is represented by the limited size (less than 20 mm in this particular case) of the samples that can be investigated. To obtain a satisfactory resolution, a scanning time of approximately one to two hours is required. Thus, no changes in the concrete can be recorded in the early stages of concrete hardening. This size also limits the maximum diameter of aggregate, which should be 5–10 times less than the sample size. Therefore, scanning concrete is more challenging in contrast to cement paste, where there is no aggregate and the particles are much smaller. These aspects significantly affect the results and should be taken into consideration in future investigations.

Acknowledgments: This work was supported by the National Centre of Science, Poland (grant No. 2014/15/D/ST8/00550 "Evaluation of the Interlayer Bond of Variably Thick Concrete Layers Based on Nondestructive Tests Using Artificial Intelligence").

Author Contributions: L.S. and D.S. conceived and designed the experiments; D.S. performed the experiments; L.S. and D.S. analyzed the data; L.S. contributed materials; L.S. and D.S. wrote the paper.

Conflicts of Interest: The authors declare no conflict of interest. The founding sponsors had no role in the design of the study; in the collection, analyses, or interpretation of data; in the writing of the manuscript; or in the decision to publish the results.

References

1. Gardziejczyk, W.; Gierasimiuk, P.; Motylewicz, M. Noisiness of the surfaces on low-speed roads. *Coatings* **2016**, *6*. [CrossRef]
2. Nasrollahi, A.; Deng, W.; Rizzo, P.; Vuotto, A.; Vandenbossche, J.M. Nondestructive testing of concrete using highly nonlinear solitary waves. *Nondestruct. Test. Eval.* **2016**, 1–19. [CrossRef]
3. Climent, M.Á.; Carmona, J.; Garcés, P. Graphite–Cement Paste: A new coating of reinforced concrete structural elements for the application of electrochemical anti-corrosion treatments. *Coatings* **2016**, *6*. [CrossRef]
4. Courard, L. Parametric study for the creation of the interface between concrete and repairs products. *Mater. Struct.* **2000**, *33*, 65–72. [CrossRef]
5. Czarnecki, L.; Chmielewska, B. Factors affecting adhesion in building joints. *Cem. Wapno Beton* **2005**, *2*, 74–85.
6. Bissonnette, B.; Courard, L.; Garbacz, A. *Concrete Surface Engineering*; CRC Press: Boca Raton, FL, USA, 2015.
7. Sadowski, Ł.; Stefaniuk, D.; Hoła, J. The porosity of concrete within the interfacial zone between layers. *Cem. Concr. Res.* **2017**. under review.
8. Ghazy, A.; Bassuoni, M.T.; Shalaby, A. Nano-modified fly ash concrete: A Repair Option for Concrete Pavements. *ACI Mater. J.* **2016**, *113*. [CrossRef]
9. Rizzo, P.; Nasrollahi, A.; Deng, W.; Vandenbossche, J. Detecting the Presence of High Water-to-Cement Ratio in Concrete Surfaces Using Highly Nonlinear Solitary Waves. *Appl. Sci.* **2016**, *6*. [CrossRef]
10. Alanazi, H.; Yang, M.; Zhang, D.; Gao, Z.J. Bond strength of PCC pavement repairs using metakaolin-based geopolymer mortar. *Cem. Concr. Compos.* **2016**, *65*, 75–82. [CrossRef]
11. Dittmer, T.; Beushausen, H. The effect of coarse aggregate content and size on the age at cracking of bonded concrete overlays subjected to restrained deformation. *Constr. Build. Mater.* **2014**, *69*, 73–82. [CrossRef]
12. Gheitasi, A.; Harris, D.K.; Muñoz, M.A.C.; Rush, S.V.; Ahlborn, T.M. The Challenges Related to Interface Bond Characterization of Ultra-High-Performance Concrete with Implications for Bridge Rehabilitation Practices. *Adv. Civ. Eng. Mater.* **2016**, *4*, 75–101.
13. Shin, H.C.; Wan, Z. Interfacial properties between new and old concretes. In Proceedings of the Second International Conference on Sustainable Construction Materials and Technologies, Ancona, Italy, 28–30 June 2010.
14. Yıldırım, G.; Sahmaran, M.; Al-Emam, M.K.M.; Hameed, R.K.H.; Al-Najjar, Y.; Lachemi, M. Effects of Compressive Strength, Autogenous Shrinkage, and Testing Methods on Bond Behavior of High-Early-Strength Engineered Cementitious Composites. *ACI Mater. J.* **2015**, *112*, 409–418. [CrossRef]
15. Sadowski, Ł.; Mathia, T.G. Multi-scale metrology of concrete surface morphology: Fundamentals and specificity. *Constr. Build. Mater.* **2016**, *113*, 613–621. [CrossRef]
16. Sierra-Beltran, M.G.; Jonkers, H.M.; Schlangen, E. Characterization of sustainable bio-based mortar for concrete repair. *Constr. Build. Mater.* **2014**, *67*, 344–352. [CrossRef]
17. Kubiak, K.J.; Wilson, M.C.T.; Mathia, T.G.; Carval, P. Wettability versus roughness of engineering surfaces. *Wear* **2011**, *271*, 523–528. [CrossRef]
18. Wojciechowski, L.; Kubiak, K.J.; Mathia, T.G. Roughness and wettability of surfaces in boundary lubricated scuffing wear. *Tribol. Int.* **2016**, *93*, 593–601. [CrossRef]
19. Kubiak, K.J.; Mathia, T.G.; Wilson, M.C.T. Methodology for metrology of wettability versus roughness of engineering surfaces. In Proceedings of the Fourteenth International Congress of Metrology, Paris, France, 22–25 June 2009.
20. Lukovic, M.; Ye, G. Effect of Moisture Exchange on Interface Formation in the Repair System Studied by X-ray Absorption. *Materials* **2015**, *9*. [CrossRef]
21. Zhou, J.; Ye, G.; van Breugel, K. Cement hydration and microstructure in concrete repairs with cementitious repair materials. *Constr. Build. Mater.* **2016**, *112*, 765–772. [CrossRef]
22. Beushausen, H.; Höhlig, B.; Talotti, M. The influence of substrate moisture preparation on bond strength of concrete overlays and the microstructure of the OTZ. *Cem. Concr. Res.* **2017**, *92*, 84–91. [CrossRef]

23. Santos, P.; Julio, E. Correlation between concrete-to-concrete bond strength and the roughness of the substrate surface. *Constr. Build. Mater.* **2007**, *21*, 1688–1695. [CrossRef]
24. Julio, E.; Branco, F.; Silva, V. Concrete-to-concrete bond strength. Influence of the roughness of the substrate surface. *Constr. Build. Mater.* **2004**, *18*, 675–681. [CrossRef]
25. Santos, P.; Júlio, E. Factors affecting bond between new and old concrete. *ACI Mater. J.* **2011**, *108*, 449–456.
26. Pan, X.; Shi, Z.; Shi, C.; Ling, T.C.; Li, N. A review on concrete surface treatment Part I: Types and mechanisms. *Constr. Build. Mater.* **2017**, *132*, 578–590. [CrossRef]
27. Garbacz, A.; Górka, M.; Courard, L. Effect of concrete surface treatment on adhesion in repair systems. *Mag. Concr. Res.* **2005**, *57*, 49–60. [CrossRef]
28. Garbacz, A.; Piotrowski, T.; Courard, L.; Kwaśniewski, L. On the evaluation of interface quality in concrete repair system by means of impact-echo signal analysis. *Constr. Build. Mater.* **2017**, *134*, 311–323. [CrossRef]
29. Hoła, J.; Sadowski, Ł.; Reiner, J.; Stach, S. Usefulness of 3D surface roughness parameters for nondestructive evaluation of pull-off adhesion of concrete layers. *Constr. Build. Mater.* **2015**, *84*, 111–120. [CrossRef]
30. Stolz, C.M.; Masuero, A.B.; Pagnussat, D.T.; Kirchheim, A.P. Influence of substrate texture on the tensile and shear bond strength of rendering mortars. *Constr. Build. Mater.* **2016**, *128*, 298–307. [CrossRef]
31. Halicka, A.; Franczak, D. Development of adhesion between two concretes during concrete hardening (in Polish). *Bud. Archit.* **2009**, *5*, 5–16.
32. Jenni, A.; Holzer, L.; Zurbriggen, R.; Herwegh, M. Influence of polymers on microstructure and adhesive strength of cementitious tile adhesive mortars. *Cem. Concr. Res.* **2005**, *35*, 35–50. [CrossRef]
33. Xiong, G.; Liu, J.; Li, G.; Xie, H. A way for improving interfacial transition zone between concrete substrate and repair materials. *Cem. Concr. Res.* **2002**, *32*, 1877–1881. [CrossRef]
34. Xiong, G.; Luo, B.; Wu, X.; Li, G.; Chen, L. Influence of silane coupling agent on quality of interfacial transition zone between concrete substrate and repair materials. *Cem. Concr. Compos.* **2006**, *28*, 97–101. [CrossRef]
35. Sahmaran, M.; Yücel, H.; Yildirim, G.; Al-Emam, M.; Lachemi, M. Investigation of the bond between concrete substrate and ECC overlays. *J. Mater. Civ. Eng.* **2013**, *26*, 167–174. [CrossRef]
36. Tayeh, B.A.; Bakar, B.A.; Johari, M.M.; Voo, Y.L. Mechanical and permeability properties of the interface between normal concrete substrate and ultra high performance fiber concrete overlay. *Constr. Build. Mater.* **2012**, *36*, 538–548. [CrossRef]
37. Tayeh, B.A.; Abu Bakar, B.H.; Megat Johari, M.A.; Zeyad, A.M. Microstructural analysis of the adhesion mechanism between old concrete substrate and UHPFC. *J. Adhes. Sci. Technol.* **2014**, *28*, 1846–1864. [CrossRef]
38. Tayeh, B.A.; Bakar, B.A.; Johari, M.M.; Ratnam, M.M. The relationship between substrate roughness parameters and bond strength of ultra high-performance fiber concrete. *J. Adhes. Sci. Technol.* **2013**, *27*, 1790–1810. [CrossRef]
39. Tayeh, B.A.; Bakar, B.A.; Johari, M.M. Characterization of the interfacial bond between old concrete substrate and ultra high performance fiber concrete repair composite. *Mater. Struct.* **2013**, *46*, 743–753. [CrossRef]
40. Carbonell Muñoz, M.A.; Harris, D.K.; Ahlborn, T.M.; Froster, D.C. Bond performance between ultrahigh-performance concrete and normal-strength concrete. *J. Mater. Civ. Eng.* **2013**, *26*. [CrossRef]
41. Luković, M.; Šavija, B.; Dong, H.; Schlangen, E.; Ye, G. Micromechanical study of the interface properties in concrete repair systems. *J. Adv. Concr. Technol.* **2014**, *12*, 320–339. [CrossRef]
42. Parisatto, M.; Dalconi, M.C.; Valentini, L.; Artioli, G.; Rack, A.; Tucoulou, R.; Ferrari, G. Examining microstructural evolution of Portland cements by in-situ synchrotron micro-tomography. *J. Mater. Sci.* **2015**, *50*, 1805–1817. [CrossRef]
43. Liskiewicz, T.; Kubiak, K.; Comyn, T. Nano-indentation mapping of fretting-induced surface layers. *Tribol. Int.* **2016**. [CrossRef]
44. Naveed, M.; Obrosov, A.; Zak, A.; Dudzinski, W.; Volinsky, A.A.; Weiß, S. Sputtering Power Effects on Growth and Mechanical Properties of Cr2AlC MAX Phase Coatings. *Metals* **2016**, *6*. [CrossRef]
45. Kubiak, K.J.; Bigerelle, M.; Mathia, T.G.; Dubois, A.; Dubar, L. Dynamic evolution of interface roughness during friction and wear processes. *Scanning* **2014**, *36*, 30–38. [CrossRef] [PubMed]
46. He, Y.; Mote, J.; Lange, D.A. Characterization of microstructure evolution of cement paste by micro computed tomography. *J. Cent. South Univ.* **2013**, *20*, 1115–1121. [CrossRef]
47. Helfen, L.; Dehn, F.; Mikulik, P.; Baumbach, T. Three-dimensional imaging of cement microstructure evolution during hydration. *Adv. Cem. Res.* **2005**, *17*, 103–111. [CrossRef]

48. Sun, W.; Wu, A.; Hou, K.; Yang, Y.; Liu, L.; Wen, Y. Experimental Study on the Microstructure Evolution of Mixed Disposal Paste in Surface Subsidence Areas. *Minerals* **2016**, *6*. [CrossRef]
49. Stock, S.R. Recent advances in X-ray microtomography applied to materials. *Int. Mater. Rev.* **2008**, *53*, 129–181. [CrossRef]
50. Rajczakowska, M.; Stefaniuk, D.; Łydżba, D. Microstructure characterization by means of X-ray micro-CT and nanoindentation measurements. *Studia Geotech. Mech.* **2015**, *37*, 75–84. [CrossRef]
51. Wieczorowski, M.; Gapinski, B. X-ray CT in metrology of geometric feature. *Acta Techn. Corviniensis-Bull. Eng.* **2014**, *7*, 95.
52. Qsymah, A.; Sharma, R.; Yang, Z.; Margetts, L.; Mummery, P. Micro X-ray computed tomography image-based two-scale homogenisation of ultra high performance fibre reinforced concrete. *Constr. Build. Mater.* **2017**, *130*, 230–240. [CrossRef]
53. Cnudde, V.; Cwirzen, A.; Masschaele, B.; Jacobs, P.J.S. Porosity and microstructure characterization of building stones and concretes. *Eng. Geol.* **2009**, *103*, 76–83. [CrossRef]
54. Du Plessis, A.; Olawuyi, B.J.; Boshoff, W.P.; Le Roux, S.G. Simple and fast porosity analysis of concrete using X-ray computed tomography. *Mater. Struct.* **2016**, *49*, 553–562. [CrossRef]
55. Ponikiewski, T.; Katzer, J.; Bugdol, M.; Rudzki, M. Determination of 3D porosity in steel fibre reinforced SCC beams using X-ray computed tomography. *Constr. Build. Mater.* **2014**, *68*, 333–340. [CrossRef]
56. Bywalski, C.; Rajczakowska, M.; Sadowski, Ł. Barrage lock concrete porosity evaluation using X-ray microtomography. *Key Eng. Mater.* **2015**, *662*, 161–164. [CrossRef]
57. Ponikiewski, T.; Katzer, J.; Bugdol, M.; Rudzki, M. Steel fibre spacing in self-compacting concrete precast walls by X-ray computed tomography. *Mater. Struct.* **2015**, *48*, 3863–3874. [CrossRef]
58. Leite, M.B.; Monteiro, P.J.M. Microstructural analysis of recycled concrete using X-ray microtomography. *Cem. Concr. Res.* **2016**, *81*, 38–48. [CrossRef]
59. Kim, K.Y.; Yun, T.S.; Park, K.P. Evaluation of pore structures and cracking in cement paste exposed to elevated temperatures by X-ray computed tomography. *Cem. Concr. Res.* **2013**, *50*, 34–40. [CrossRef]
60. Feldkamp, L.A.; Davis, L.C.; Kress, J.W. Practical cone-beam algorithm. *J. Opt. Soc. Am.* **1984**, *1*, 612–619. [CrossRef]
61. Różański, A.; Rajczakowska, M.; Serwicki, A. The influence of microstructure geometry on the scale effect in mechanical behaviour of heterogeneous materials. *Sci. Eng. Compos. Mater.* **2015**. [CrossRef]
62. Gallucci, E.; Scrivener, K.; Groso, A.; Stampanoni, M.; Margaritondo, G. 3D experimental investigation of the microstructure of cements pastes using synchrotron X-ray microtomography (μCT). *Cem. Concr. Res.* **2007**, *37*, 360–368. [CrossRef]
63. Bernardes, E.E.; Carrasco, E.V.M.; Vasconcelos, W.L.; de Magalhães, A.G. X-ray microtomography (μ-CT) to analyze the pore structure of a Portland cement composite based on the selection of different regions of interest. *Constr. Build. Mater.* **2015**, *95*, 703–709. [CrossRef]